Statistical downscaled local climate model for future rainfall changes analysis: A case study of Hyogo prefecture, Japan

Ng P.Y.[1], Tan K.W.[1]*, Satoru O.[3] and Huang Y.F.[2]
[1]Faculty of Engineering and Green Technology, Universiti Tunku Abdul Rahman, 31900, Kampar, Perak, Malaysia.
[2]Lee Kong Chian Faculty of Engineering and Science, Universiti Tunku Abdul Rahman, 43000 Kajang, Selangor, Malaysia.
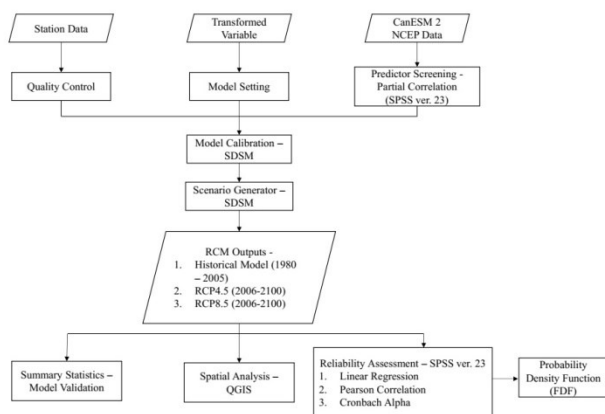[3]Research Centre for Urban Safety and Security, Kobe University, Nada-ku, Kobe 657-8501, Japan
*to whom all correspondence should be addressed: e-mail: tankokweng@utar.edu.my

Graphical abstract

1. Introduction

Climate change can be seen from the rise in global annual temperature and the increase in extreme event occurring frequency worldwide throughout the years. The global averaged temperature in 2020 was reported to be 1.02 ℃ higher than the baseline period of the year 1951 – 1980 and tied with 2016 as the hottest year ever recorded (NASA, 2021). According to Pidcock and McSweeney (2021), 79% of extreme weather event cases were found to have their likelihood or severity altered due to human-caused climate change, where 70% were made more likely or severe, and 9% were made less likely or severe. As the increased severity of extreme weather events caused by human actions is higher in proportion, more focus should be given to the human activities that are more controllable compared to natural causes.

The main factor causing climate change is the greenhouse effect, where greenhouse gas (GHG) traps solar heat and prevents it from escaping into the space, thus leading to global warming. There are two types of greenhouse gas emission sources, which are natural processes and anthropogenic activities. However, climate change due to human activities has become the most serious of all environmental concerns (Mikhaylov *et al.*, 2020). Human activities such as deforestation and burning fossil fuels for electric generation emit carbon dioxide, leading to global warming and climate change.

The climate model could be understood as a more comprehensive weather model. It predicts over an extended period of time and forecasts how conditions in a region will alter over the following decades. Climate modelling is used in understanding the future trend of climate systems, and it allows scientists to test hypotheses and predict future climates. Also, model output helps scientists comprehend how human activity influences Earth's climate. General climate models (GCMs) are sophisticated mathematical descriptions of key components of climate systems, such as atmosphere,

Abstract

For decades, climate models have been used to understand the present and historical climates, especially global climate models (GCMs). They are used to understand the interaction between climate system processes and forecast future climates. However, the issue of low resolution and accuracy often lead to inadequacy in capturing the variations in climate variables related to impact assessment. In order to capture the local climate changes in Hyogo Prefecture of Western Japan, a local climate modelling based on Second Generation Canadian Earth System Model (CanESM2) was applied using the statistical downscaling technique. Representative Concentration Pathway (RCP) 4.5 and 8.5 scenario were used in generating future climate models. The reliability of models was tested with linear regression, Pearson correlation, and Cronbach Alpha. Moderate relationship between rainfall data and both RCP scenarios was found in all chosen stations. Spatial analysis outcome showed that there is a possibility of increase in annual rainfall in Hyogo prefecture, where the increase is significant in Northern region. There is a possibility of increase in maximum and minimum temperature in four selected stations due to the increase of greenhouse gas emissions.

Ng P.Y., Tan K.W., Satoru O. and Huang Y.F. (2023), Statistical downscaled local climate model for future rainfall changes analysis: A case study of hyogo prefecture, japan, *Global NEST Journal*, **25**(5), 136-146.

ocean, land surface and sea ice, and the interactions between them. However, the resolution and accuracy of GCMs, which are low, are often inadequate to record the climate variable variations, especially in impact assessments. Raw data from GCMs is difficult to be applied at local scales without downscaling due to its coarse resolution. Downscaling allows identification and analysis of extreme events, which are significant components of urban climate study (Domínguez *et al.*, 2013). Regional climate models (RCMs) are the products of downscaling,

which have improved spatial and temporal resolution of the parent global models. Besides, lack of scientific studies was conducted to assess the performance of RCMs in Hyogo Prefecture, Japan based on two potential emission scenarios - Representative Concentration Pathways (RCPs) 4.5 and 8.5. Hence, the findings of this study will benefit society as future climate conditions are able to be predicted through the statistical downscaling method.

Table 1. Population growth of selected cities and towns in 1995 – 2020

City/Town	Land Area (km2)	Growth Rate (%) 1995-2020*	Population Density 2020* (/km²)
Toyooka City	697.55	-17.41	111.13
Taka Town	185.19	-24.20	104.13
Sanda City	210.32	13.55	519.80
Kobe City	557.01	7.25	2741.46
Tatsuno City	210.87	-10.88	352.61
Yabu City	422.91	-29.25	52.34
Fukusaki Town	45.79	-2.41	423.15
Kamigoori Town	150.26	-26.26	92.48
Total (Hyogo)	8,400.94	-	-

Growth rate and population density in 2020 were calculated from the obtained data.

Table 2. Selected rainfall stations during 1980 – 2020

City/Town	Station name	Latitude	Longitude	Period
Toyooka City	Tsuji	35.5194 N	134.7528 E	1980 - 2020
Taka Town	Sugihara	35.1375 N	134.9214 E	1980 - 2020
Sanda City	Sanda	34.8950 N	135.2117 E	1980 - 2020
Kobe City	Rokkousabou	34.7158 N	135.2650 E	1980 - 2020
Fukusaki Town	Fukusaki	34.9500 N	134.7483 E	1980 - 2020
Tatsuno City	Nishikurisu	34.9567 N	134.4658 E	1980 - 2020
Yabu City	Deai	35.3636 N	134.5947 E	1980 - 2020

2. Materials and methods

2.1. Study area

Hyogo Prefecture is located in Kansai Region in Japan, having Kobe as the capital. There are 29 cities (*shi*) and 12 towns (*cho*) in Hyogo prefecture. It has a total land area of 8,400.95 km^2 and a total population of 5,466,000 as of 2019. Kobe is the largest city located in Hyogo Prefecture and has Port of Kobe as one of the chief ports in Japan. Port of Kobe was established in the first year of the Meiji era, 1868, and eventually became an international trading hub to Asia countries.

The populations in several cities and towns in Hyogo Prefecture were obtained from Hyogo Prefectural Government and Statistics Bureau of Japan (https://web.pref.hyogo.lg.jp/ and www.stat.go.jp), and the population growth was then calculated. It could be observed from Table 1 that the population in cities/towns, except Sanda City and Kobe City, decreased over 25 years, with the highest negative growth rate value of -24.20%. Kobe City had the highest population density in 2020, which was 2741.46 /km^2.

2.2. Data collection

Seven rainfall stations in Hyogo Prefecture were selected which covered different regions of Hyogo Prefecture. Total

41 years of daily rainfall (1980 – 2020) were downloaded from Water Information System and Japan Meteorological Agency online portal (http://www1.river.go.jp/ and https://www.jma.go.jp/jma/
indexe.html). The detail and the location of stations were shown in Figure 1 and Table 2.

To develop temperature local climate model, the daily minimum temperature (T_{min}) and maximum temperature (T_{max}) data from selected four stations (1980- 2020) were used in this study, which covered the northern, south-eastern, southern and south-western regions of Hyogo Prefectures. The stations were shown in Table 3 and Figure 2. The data set were used for model calibration and validation using Statistically Downscaling Model (SDSM) ver. 4.6. Theoretically, 30-year observation data was suggested to calibrate the model, while total 41 years data (1980-2020) were used in this study to obtain higher accuracy in calibration. Then, the reliability analysis period of observed daily rainfall, T_{min} and T_{max}. which was set as 2006 – 2020, from the same stations were obtained and used to determine the suitable local climate models.

The second-generation Canadian Earth System Model (CanESM2) was used to develop the local climate models. It was developed by Canadian Centre for Climate Modelling and Analysis (CCCma) and recognised as fourth generation of CGCM, which contributes to the IPCC AR5 and takes part

in CMIP5. The main components of Earth System Model include an atmospheric, an oceanic, a sea-ice and two land surface models, namely Atmospheric General Circulation Model (AGCM4), Ocean GCM4, CanSim1, CTEM1 and Canadian Land Surface Scheme (CLASS2.7). The GCM CanESM2 was downloaded from online portal (https://climate-scenarios.canada.ca/?page=pred-canesm2). The downloaded CanESM2 dataset consisted the predictors (1961_2005), historical model (1961 – 2005) and climate projection period (2006 – 2100) based on RCP4.5 and 8.5 scenario. Hyogo Prefecture is located at grid cell BOX_49X_45Y defined by CanESM2 as shown in Figure 3. The 26 predictors and their codes are listed in Table 4. The RCP4.5 and RCP8.5 were utilised in this study to generate future scenarios of anthropogenic forcing under intermediate and high emission levels. Besides, the rainfall intensity of historical flood events that occurred in Toyooka City, Kobe City, Taka Town and Tatsuno City were collected. The data were arranged and plotted accordingly with the moving average.
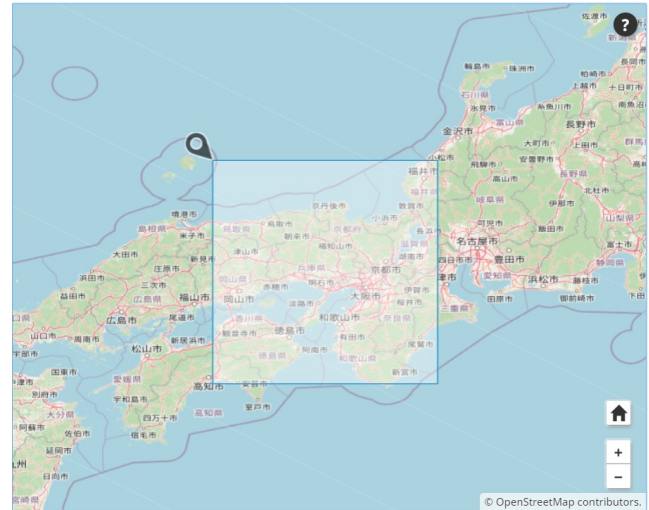

Figure 3. Grid cell (box) covering Hyogo Prefecture (Government of Canada, n.d.)

Table 4. The 26 predictors from NCEP

No	File name	Predictor Name	No	File Name	Predictor Name
1	P*mslpgl.dat	Mean sea level pressure	14	P*p5zhgl.dat	500 hPa Divergence of true wind
2	P*p1_fgl.dat	1000 hPa Wind speed	15	P*p850gl.dat	850 hPa Geopotential
3	P*p1_ugl.dat	1000 hPa Zonal wind component	16	P*p8_fgl.dat	850 hPa Wind speed
4	P*p1_vgl.dat	1000 hPa Meridional wind component	17	P*p8_ugl.dat	850 hPa Zonal wind component
5	P*p1_zgl.dat	1000 hPa Relative vorticity of true wind	18	P*p8_vgl.dat	850 hPa Meridional wind component
6	P*p1thgl.dat	1000 hPa Wind direction	19	P*p8_zgl.dat	850 hPa Relative vorticity of true wind
7	P*p1zhgl.dat	1000 hPa Divergence of true wind	20	P*p8thgl.dat	850 hPa Wind direction
8	P*p500gl.dat	500 hPa Geopotential	21	P*p8zhgl.dat	850 hPa Divergence of true wind
9	P*p5_fgl.dat	500 hPa Wind speed	22	P*prcpgl.dat	Total precipitation
10	P*p5_ugl.dat	500 hPa Zonal wind component	23	P*s500gl.dat	500 hPa Specific humidity
11	P*p5_vgl.dat	500 hPa Meridional wind component	24	P*s850gl.dat	850 hPa Specific humidity
12	P*p5_zgl.dat	500 hPa Relative vorticity of true wind	25	P*shumgl.dat	1000 hPa Specific humidity
13	P*p5thgl.dat	500 hPa Wind direction	26	P*tempgl.dat	Air temperature at 2 m

Figure 1. Selected rainfall stations plotted in map.

Table 3. Selected stations for minimum temperature and maximum temperature for year 1980 – 2020

Station name	Latitude	Longitude	Time Period
Toyooka	35.5350 N	134.8217 E	1980 - 2020
Sanda	34.8950 N	135.2117 E	1980 - 2020
Fukusaki	34.9500 N	134.7483 E	1980 - 2020
Kamigoori	34.8583 N	134.3733 E	1980 - 2020

Figure 2. Selected stations for minimum and maximum temperatures plotted in map

2.3. Downscaling procedure

Quality control was first performed to identify the missing data, where missing daily precipitation amount, minimum and maximum temperature data were treated by getting the data from nearest station available. It is important to undergo quality control step, as missing data leads to reduction in statistical power, which means it will decrease the probability that the null hypothesis of the test will be rejected when it is false (Kang, 2013). Besides, it has the potential to decrease sample representativeness. Absence of data also causes biasness in the parameter estimation. Thus, it is important to treat the data before undergoing further steps.

After obtaining observed rainfall, minimum (Tmin.) and maximum temperature (Tmax.) data of the stations, the predictors were screened. Screening is the process of selecting variables that favourably includes or eliminates certain characteristics of the predictor-predictand relationship (Delsole and Shukla, 2009). Predictands, which

are the observed historical readings, were screened with all 26 predictors. Predictors with significance level lower than 0.05 and R-squared value close to 1 were chosen. The primary null hypothesis of multiple regression is "there is no relationship between the independent (X) variables and the dependent (Y) variables" (McDonald, 2014). Thus, when the significance level is lower than 0.05 (5%), the null hypothesis is rejected, meaning there is lower than 5% probability that there is no relationship between the independent and dependence variables. Whereas the R-squared (R^2) value defines how well the regression line fits into the data, ranging from 0 to 1. When the R^2 is 1, it means 100% of the variation in dependent variable could be explained by the independent variable. The sets of predictor variables that are most appropriate were selected.

After predictor screening, model calibration was performed using Statistical DownScaling Model (SDSM) ver. 4.6. The observed data of 1980 – 2005 were used as predictand and the predictor datasets obtained in predictor screening were used for model calibration. The 1980 – 2005 period was selected due to the availability of station data and the past climate conditions available for historical simulated model from CanESM2. The projection period was determined based on the RCP scenarios, which are 2006 – 2100. The stochastic weather generator was used to produce the ensembled models which were historical model (1980-2020). The historical model was validated by comparing observation data (1980 – 2005) using the summary statistics – monthly maximum, minimum and average value of rainfall, Tmax. and Tmin.

The local climate models (RCP4.5 and 8.5) were bias corrected using delta method. Although there is significant variance spatially and temporally in different bias correction approaches, the delta method outperforms the other two methods on average in minimizing the median absolute error between debiased simulation and empirical data for precipitation and temperature (Beyer, Krapp and Manica, 2019). Therefore, delta method was performed to the simulated rainfall data. Several assumptions must be made in this method, whereby the biases between simulated data and present observation remain unchanged over time, and the bias is specific to the location (Maraun and Widmann, 2018). Multiplicative bias correction for precipitation is more suitable rather than additive when using delta method (Maraun and Widmann, 2018). Thus, the equation for debiased precipitation used is as follows:

$$P'_{sim}(t) = P_{sim}(t) \times \frac{P_{obs}(0)}{P_{sim}(0)} = P_{obs}(0) \times \frac{P_{sim}(t)}{P_{sim}(0)}$$

2.4. Statistical analysis

The Pearson correlation (r), linear regression (R^2), Cronbach's Alpha were applied to assess the reliability of the local climate models. Pearson correlation analysis was first applied to determine the connection strength between two variables, where its degree of association could be determined by correlation coefficient "r", also known as Pearson's correlation coefficient. In other words,

it is the measure of linear correlation strength and direction between two data sets.

Pearson correlation coefficient ranges between -1 to +1, where +1 indicates that the independent and dependent variables are positively and linearly related; while -1 indicates that they are perfectly related in positive and linear manner (Gogtay and Thatte, 2017). The zero-coefficient value indicated the absence of linear relationship between the independent and dependent variable. The relationships between observation and model were assumed to be linear and are independent of each other. Hence, the correlation coefficient was set as r $\geq$ 0.5 which indicated the acceptable correlation.

Linear regression line is represented in the form $Y=a+bX$, where X - independent variable, Y - dependent variable, b - slope of line and a - y-intercept. This regression measures the goodness of fit between two (independent and dependent) variables linearly. The R-squared (R^2) coefficient ranged between 0 – 1.00. Thus, the higher the value of R-squared, the better the observations could be fitted by the regression model (Frost, 2021). In this study. the R^2 coefficient was set as $\geq$ 0.4, which indicated acceptable level between model and observation data points the acceptable level. In linear regression models, there assumptions were made in this study. Firstly, the relationship between independent variable (X) and the mean of dependent variable (Y) must be linear. Secondly, the models generated were homoscedastic, which the error variance was independent of predictor's values. Lastly, the dependent variable was assumed to be normally distributed for any fixed value of independent variable.

The Cronbach's Alpha enabled the estimation of internal consistency of a specific test, in other words, the degree to which a group of items are closely related. It is also regarded as an indicator for scale reliability. The Cronbach's Alpha can be calculated using the following formula:

$$\alpha = \frac{N\bar{c}}{\bar{v} + (N-1)\bar{c}}$$

Where, N represents the number of items, $\bar{c}$ is the covariance between elements on an average basis and $\bar{v}$ represents the averaged variance (UC Regents, 2021). The Cronbach's Alpha was used to determine the fraction of variance in the set of test results. It ranged between 0.00 to 1.00 (Brown, 2002). The α value was set as 0.6-0.7 indicated acceptable level of reliability.

2.5. Spatial analysis

Spatial analysis is defined as the manipulation of existing available spatial data in order to elicit new information and meaning. It is normally done using Geographic Information System (GIS), which is a tool used to compute feature statistics and undergo geoprocessing operations, such as data interpolation. Spatial interpolation, which was used in this study, is a technique of estimating the values at other unknown sites by utilizing points with known values. Specifically, Inverse Distance Weighted (IDW) interpolation approach weighs the sample points so that the effect of the

point on the other decreases with distance from the specific unknown point of interest. (Yang, *et al.*, 2015) stated that, in terms of efficiency in computation and relative errors, IDW interpolation method showed better performance as compared to others, such as Kriging and Spline interpolation methods. Thus, IDW interpolation method was used in this study (Figure 4).
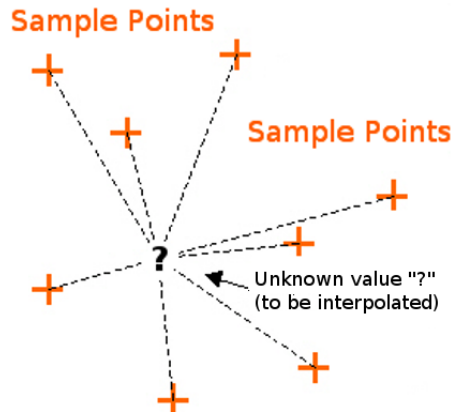

Figure 4. Inverse Distance Weighted (IDW) interpolation (Mitas and Mitasova, 1999)

The observed and rainfall models were averaged in 20 years period from 1980 to 2100. The data set were imported as Comma Separated Value (CSV) files for both RCP4.5 and RCP8.5. The study area was then traced into a polygon layer to be used as the mask layer. The IDW interpolation was done to the 20-year annual average rainfall intensity, and the intensities of unknown locations away from the stations were interpolated with the use of weighting coefficient.

3. Results and discussion

3.1. Rainfall

3.1.1. Model validation

Historical models (1980 to 2005) of rainfall were simulated using selected predictors, as shown in **Error! Reference source not found.** and validated by comparing the same period of observed rainfall data. Two predictors, 1000 hPa divergence of true wind and total precipitation, were used for simulation of local climate models for the stations except for Tsuji station. The mean and maximum value of both sets of data were compared and analyzed. As shown in Figures 5 and 6, the mean monthly rainfall shows there is minor difference between observed and simulated value for all stations. The simulated historical model consistently overestimated the average monthly rainfall by 20.4%. However, the average maximum monthly rainfall shows major differences between observed and historical models especially in the period of May – September, consistent underestimation is observed in all selected stations. This may be caused by extreme weather events, for instance, El Nino and La Nina, and Typhoon. Thus, the analysis of local climate models should include the factor of extreme weather occurrence which may cause the major outlier (Table 5).

Table 5. The predictors used for simulation of local climate models

| Station	Predictors
Tsuji	1000 hPa Relative vorticity of true wind
	1000 hPa Divergence of true wind
	850 hPa Divergence of true wind
	Total precipitation
	500 hPa Specific humidity
Sugihara	1000 hPa Divergence of true wind
	Total precipitation
Sanda	1000 hPa Divergence of true wind
	Total precipitation
Fukusaki	1000 hPa Divergence of true wind
	Total precipitation
Nishikurisu	1000 hPa Divergence of true wind
	Total precipitation
	500 hPa Specific humidity
Rokkousabou	1000 hPa Divergence of true wind
	Total precipitation
Deai	1000 hPa Divergence of true wind
	Total precipitation
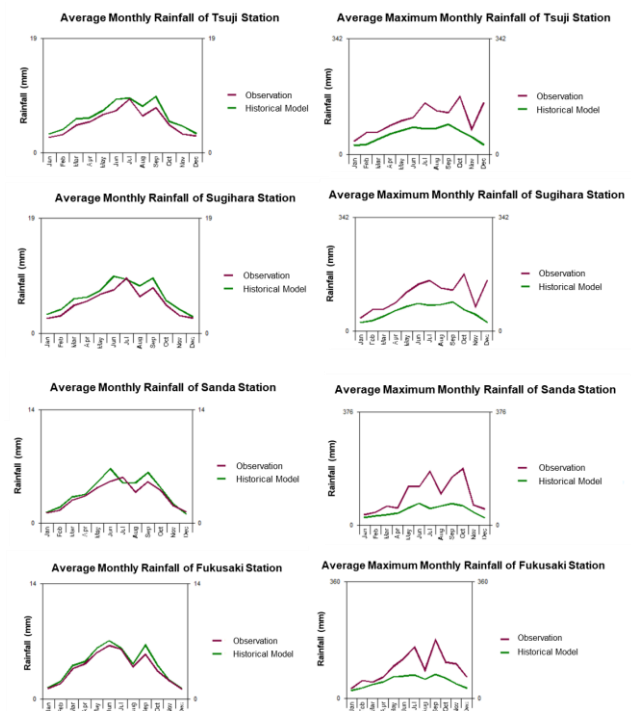
Figure 5. Comparison of observation and historical model (1980-2005) for average and maximum monthly rainfall in Tsuji, Sugihara, Sanda and Fukusaki Stations

3.1.2. Reliability assessment of local climate models (rainfall)

The reliability assessments, R-squared test, Pearson correlation test and Cronbach's Alpha were applied to determine the reliability of simulated climate models, and the results are shown in Table 6. The local climate models based on RCP4.5 and RCP8.5 scenario met the minimum predefined criteria and indicated reliable in which are observed from Fukusaki and Nishikurisu stations that were shaded. Besides, other stations show R-squared, Person correlation and Cronbach's Alpha that are above the acceptable values for RCP4.5 and RCP8.5. As stated in IPCC

(2021), all RCPs scenarios, except for RCP 2.6, projected that the warming will persist beyond 2100. Thus, local climate models based on RCP4.5 and RCP8.5 were discussed and analysed in this study because both scenarios represented the local climate condition.

Additionally, this study also compared the observed and local climate models using probability density function (PDF) to verify the variations between observation and local climate model. The local climate model of rainfall based on RCP4.5 and RCP8.5 showed similar curve and positions below the observed precipitation data curve for all rainfall stations (as Figure 7). The similar medians were obtained in all stations, except for the Tsuji Station (Table 7). However, the underestimation issue was also found based on PDF analysis outcome. Thus, the current local rainfall pattern may moderately follow RCP 4.5 and 8.5 Scenario. The associated climate change magnitudes and rates based on medium to high emission scenarios (RCP4.5, RCP6.5 and RCP8.5) would likely cause the high risk and irreversible regional changes in terms of structure, composition and function of ecosystems (IPCC, 2021).

Table 6: Reliability assessment outcome of the rainfall stations

Station	RCPs	R^2 ($R^2 \geq 0.4$)	Pearson Correlation ($r \geq 0.5$)	Cronbach's Alpha ($\alpha \geq 0.4$)
Tsuji	4.5	0.046	0.227	0.366
	8.5	0.058	0.241	0.384
Sugihara	4.5	0.365	0.605*	0.695*
	8.5	0.358	0.599*	0.699*
Sanda	4.5	0.338	0.581*	0.679*
	8.5	0.348	0.590	0.685*
Rokkousabou	4.5	0.324	0.569	0.673*
	8.5	0.328	0.573*	0.675*
Fukusaki	4.5	0.452*	0.672*	0.769*
	8.5	0.437*	0.661*	0.760*
Nishikurisu	4.5	0.471*	0.686*	0.784*
	8.5	0.448*	0.669*	0.771*
Deai	4.5	0.229	0.479	0.572*
	8.5	0.258	0.508*	0.384

Indicated the significant value

Table 7. Median of rainfall for observed, RCP4.5 and RCP8.5 model based on PDF curves

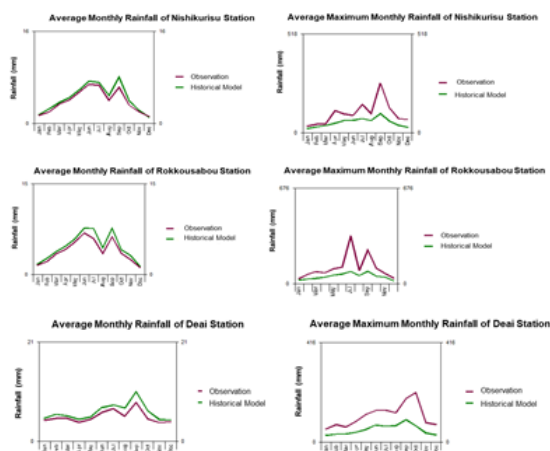| RCP Scenario Station	Rainfall (mm)		
	Observed	RCP4.5	RCP8.5
Tsuji	178.16	194.33	195.13
Sugihara	165.26	165.26	165.26
Sanda	112.63	112.63	112.63
Fukusaki	127.79	127.79	127.79
Nishikurisu	121.35	121.35	121.35
Rokkousabou	105.93	105.93	105.93
Deai	196.89	196.89	196.89

Figure 6. Comparison of observation and historical model (1980-2005) for average and maximum monthly rainfall in Nishikurisu, Rokkousabou and Deai Stations
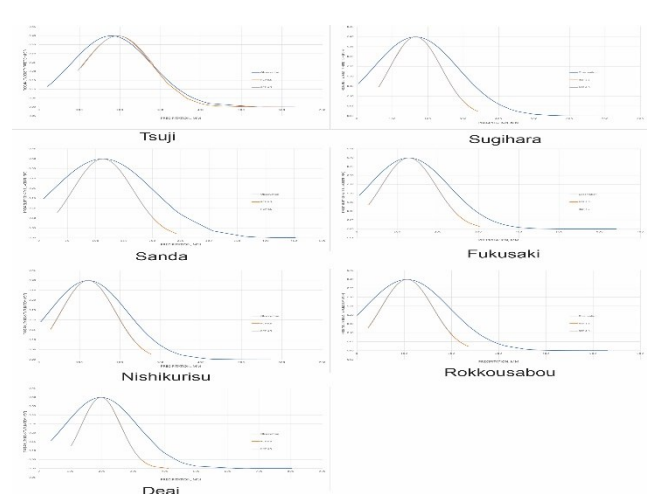

Figure 7. Probability Density Function (PDF) for observed rainfall and local climate models for different stations

3.1.3. Spatial analysis of rainfall pattern

The observed annual rainfall of Hyogo Prefecture was averaged from 1980 – 1999 and 2000 – 2020; whereas the simulated rainfall based on RCP4.5 and RCP8.5 scenarios were averaged for 2021 – 2040, 2041 – 2060, 2061 – 2080, and 2081 – 2100. These averaged annual rainfall (1980 – 2100) were analysed spatially using QGIS and the rainfall data of unknown points located within the Hyogo Prefecture were interpolated using IDW interpolation.

The Figure 8 illustrates the rainfall patterns of Hyogo Prefecture based on 41 years data (1980 to 2020). The rainfall intensity in Northern region increased from 1980 to 2020; however, the rainfall intensity in South-western and South-eastern region decreased in same period.
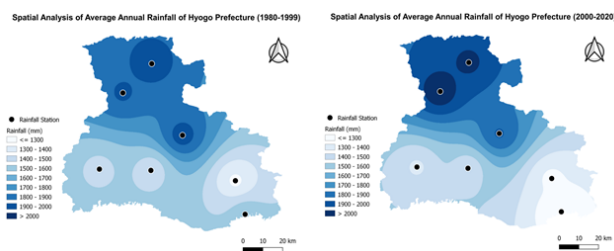
Figure 8. Annual rainfall pattern in Hyogo Prefecture based on 1980-1999 and 2000-2020 period

As shown in Figure 9, the local climate model of rainfall (2021 to 2100) based on RCP4.5 scenario for the Northern region is projected to have increase significantly. The Southern part of the study area is predicted to experience increase in rainfall in the period of 2021 – 2040 based on RCP4.5 scenario. There is minor part of Southern region is projected to experience significant fluctuation of rainfall intensity for 2021 – 2100 period.
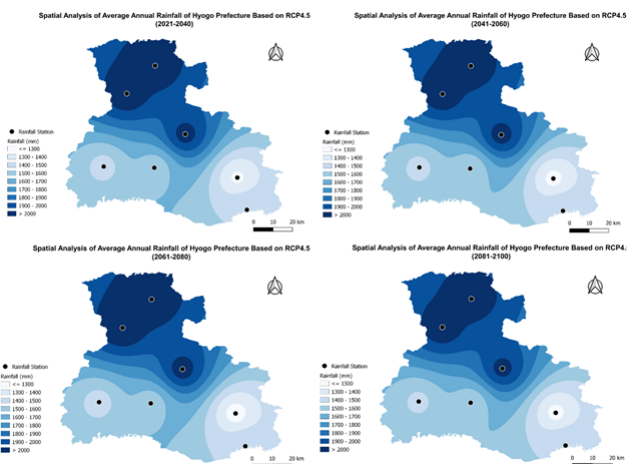

Figure 9. Simulated annual rainfall pattern in Hyogo Prefecture based on RCP4.5 (2021-2040, 2041-2060, 2061-2080 and 2081-2100)

Based on the local climate model RCP8.5 scenario (Figure 10), it indicates that greater increase in rainfall intensity as compared to RCP4.5 scenario especially the Northern region of the Hyogo Prefecture is projected to have significant increase in second quarter of 21st century (2050-2100). Besides, the Southwestern and Southeastern region of Hyogo Prefecture might experience an increase of rainfall intensity in the 2021- 2040 period, which is projected having slightly fluctuations toward to end of this century.
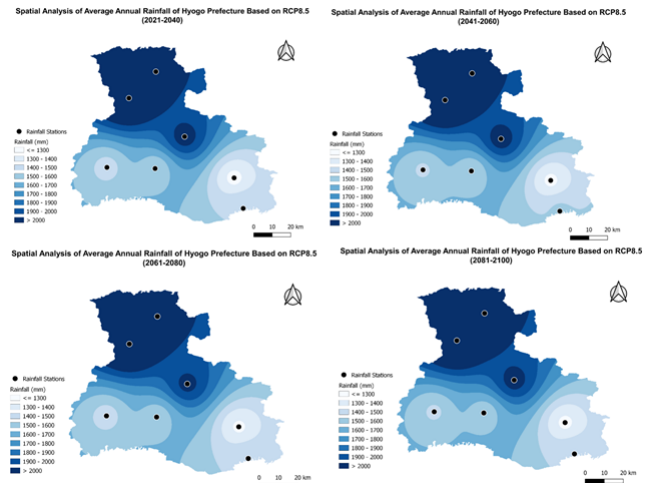

Figure 10. Simulated annual rainfall pattern in Hyogo Prefecture based on RCP8.5 in 2021-2040, 2041-2060, 2061-2080 and 2081-2100

Table 8. Predictors used for simulation of maximum and minimum temperature climate models

Stations	Predictors
Toyooka	Mean sea level pressure
	500 hPa Geopotential
	500 hPa Wind speed
	500 hPa Zonal wind component
	500 hPa Specific humidity
	850 hPa Specific humidity
	Air temperature at 2 m
Sanda	Mean sea level pressure
	500 hPa Geopotential
	500 hPa Wind speed
	500 hPa Zonal wind component
	500 hPa Specific humidity
	850 hPa Specific humidity
	Air temperature at 2 m
Fukusaki	Mean sea level pressure
	500 hPa Geopotential
	500 hPa Wind speed
	500 hPa Zonal wind component
	500 hPa Specific humidity
	850 hPa Specific humidity
	Air temperature at 2 m
Kamigoori	Mean sea level pressure
	500 hPa Geopotential
	500 hPa Wind speed
	500 hPa Zonal wind component
	500 hPa Specific humidity
	850 hPa Specific humidity
	Air temperature at 2 m

3.2. Temperature

3.2.1. Model validation

The historical models (1980 – 2005) of maximum (Tmax.) and minimum temperature (Tmin.) were simulated using the selected predictors, which are listed in Table 8. The similar predictors were loaded for all stations as mean sea

level pressure, the geopotential, wind speed, zonal wind component, specific humidity at 500 hPa pressure level, specific humidity at 850 hPa pressure level and the air temperature at 2 m. The historical models were then validated against the observed Tmax. and Tmin.. The means of both simulated model and observation were compared and analysed in this study.
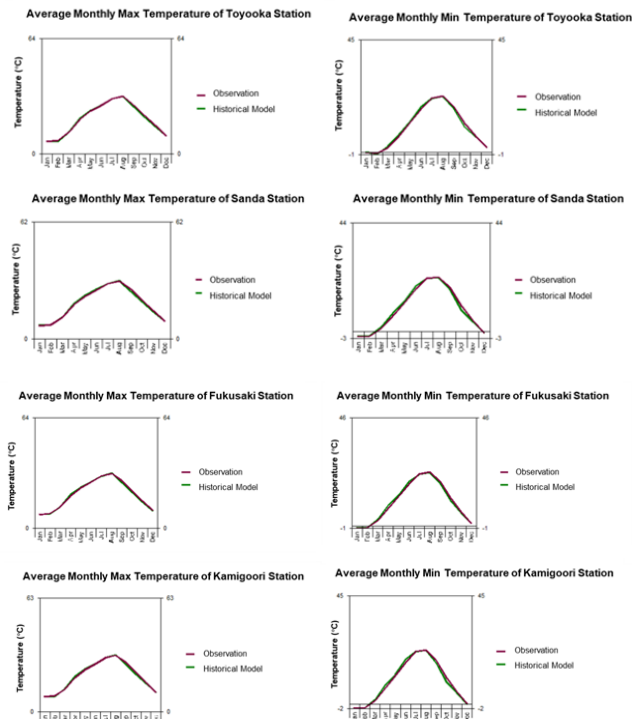

Figure 11. Comparison of observation and historical model (1980-2005) for maximum (Tmax.) and minimum temperature (Tmin.) in Fukusaki, Kamigoori, Sanda and Toyooka Stations.

Figure 11 shows the average of Tmax. and Tmin.. Similar mean of Tmax. are obtained for observation and historical models throughout the year. For Tmin., there are slightly underestimation for all stations in the October based on 1980-2005 period.

3.2.2. Reliability assessment of local climate models (temperature)

Based on the reliability assessment results (Tables 9 and 10), all stations that meet the minimum criteria and show strong reliability for both scenarios, with high R-squared, Pearson correlation and Cronbach's Alpha coefficient. Thus, both scenarios (RCP4.5 and RCP8.5) are discussed and analysed in this study. The average Tmax. and Tmin. in Toyooka station were illustrated in Figures 12 and 13. The underestimation issue is observed for Tmax. based on observed, RCP4.5 and RCP8.5 local climate model, which the highest deviation recorded as 1.1 °C. The average annual Tmin. in Toyooka for observed and local climate models (RCP4.5 and RCP8.5). Similarly, underestimation issue was found which highest deviation of 1.0 °C was observed in this study. Based on the Figures 12 and 13, increasing trends were found in the models (RCP4.5 and 8.5), however from 2066 onwards, the local climate model simulated based on RCP8.5 shows a higher Tmin. (0.4 – 1.0 ºC) compared to RCP4.5.
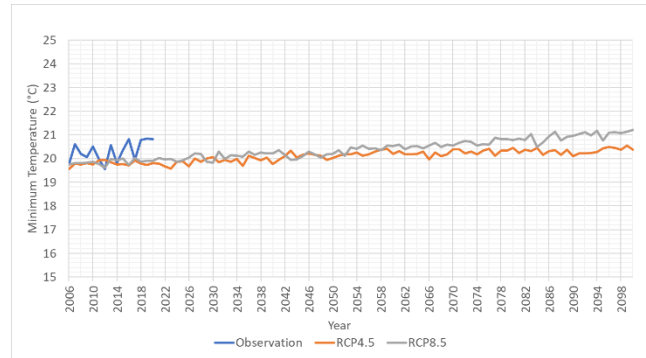

Figure 12. The observed, local climate models based on RCP4.5 and 8.5 for average maximum temperature (Tmax.) observed in Toyooka station (2006-2100)
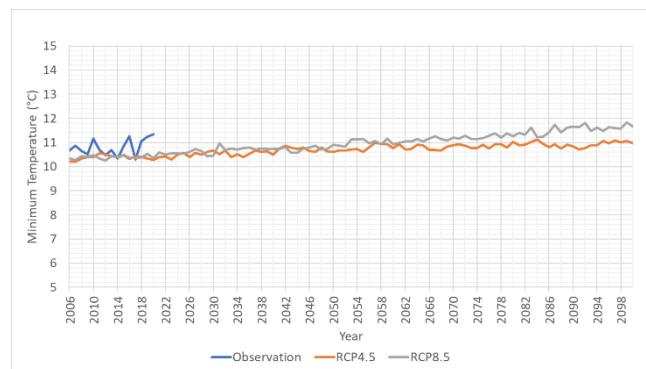

Figure 13. The observed, local climate models based on RCP4.5 and 8.5 for average minimum temperature (Tmin.) in Toyooka station (2006-2100)

The average Tmax. and Tmin. for Sanda (2006 - 2100) were determined as shown in Figures 14 and 15. The observed Tmax. recorded in Sanda station (2006 – 2020) ranges from 18.7 °C to 20.6 °C; whereas the local climate models simulated based on RCP4.5 and RCP8.5 range from 18.8 °C to 19.9 °C and 18.9 °C and 20.5 °C respectively. By comparing with the observed Tmax. recorded in Sanda station (2006 – 2020), the underestimation issue was identified with the highest deviation recorded as 1.5 °C.

In contrast, overestimate issue was identified (as Figure 15) in local climate models (Tmin.) with the highest deviation recorded as 0.9 °C. The observed Tmin. (2006 – 2020) ranges from 8.5 °C to 9.6 °C, where the local climate models simulated based on RCP4.5 and RCP8.5 range from 9.2 °C to 10.2 °C and from 9.3 °C to 11.0 °C respectively. However, the RCP8.5 model has shown the higher average Tmin. as compared to RCP4.5 model. The increase trends for Tmax. and Tmin. were observed in local climate model based on RCP4.5 and RCP8.5. Obviously, the local climate model (RCP8.5) for Tmax. show a significant increase in the third quarter of the 21st century.

Moving forward to Southern region of Hyogo Prefecture, the average Tmax. and Tmin. in Fukusaki were determined in this study. Based on Figure 16, the underestimation issue found in the simulated models based on RCP4.5 and RCP8.5 scenario with a largest deviation of 1.5 °C. The ran range of observed average Tmax. recorded as 20.3 °C to 21.5 °C; whereas the local climate model based on RCP4.5 and

RCP8.5 scenario were simulated as 19.8 °C to 20.6 °C and 19.8 °C to 21.3 °C respectively. Increase trends were also observed in the local climate models based on RCP4.5 and RCP8.5, however the RCP8.5 model shows the significant increase starting from 2058 onwards.

The simulated climate model (Tmin.) based on RCP4.5 and RCP8.5 scenario show slightly difference compared to the observed Tmin. (2006 to 2020) (Figure 17). The observed Tmin. (2006 – 2020) in Fukusaki station recorded the average Tmin. ranges from 10.2 °C to 11.3 °C; whereas the range of RCP4.5 and 8.5 scenario local model range from 10.4 °C to 11.3 °C and 10.4 °C to 12.0 °C. Nevertheless, the increase trend is also identified in the local climate model based on RCP4.5 and 8.5 scenario, however the Tmin. based on RCP8.5 scenario shows a significant increase starting from 2066 onwards.
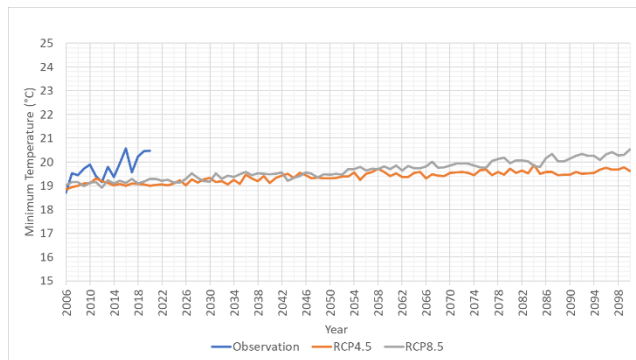

Figure 14. The observed, local climate models based on RCP4.5 and 8.5 for average maximum temperature (Tmax.) in Sanda Station (2006-2100)
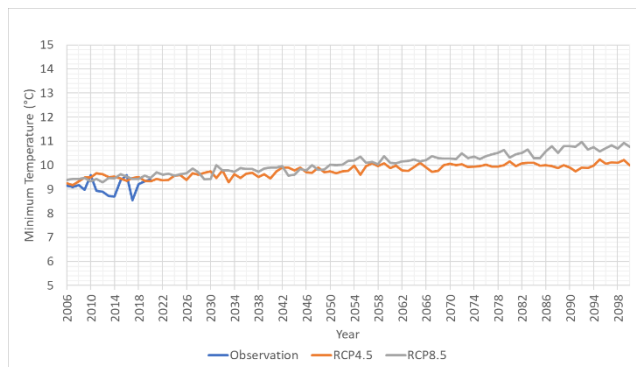

Figure 15. The observed, local climate models based on RCP4.5 and 8.5 for average minimum temperature (Tmin.) in Sanda Station (2006-2100)

Similar trend was found in South-eastern region (Kamigoori station) as shown in Figures 18 and 19. Based on the results, the range of observed Tmax. Starting from 19.9 °C to 21.0 °C. The local climate models based on RCP4.5 and 8.5 scenario show the Tmax. range from 19.8 °C to 20.7 °C, and 19.8°C - 21.3 °C respectively. The uptrend is simulated in the RCP 8.5 scenario after 2066. Similar simulation was recorded for Tmin. (Figure 19). This is due to higher emission scenario with GHGs reduction policy are not available in most of the countries after 2050.
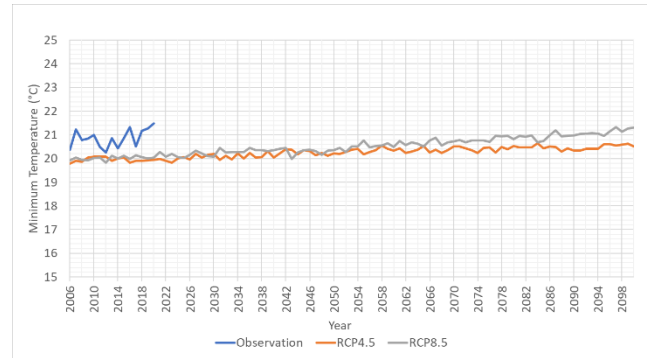

Figure 16. The observed, local climate models based on RCP4.5 and 8.5 for average maximum temperature (Tmax.) in Fukusaki Station (2006-2100)
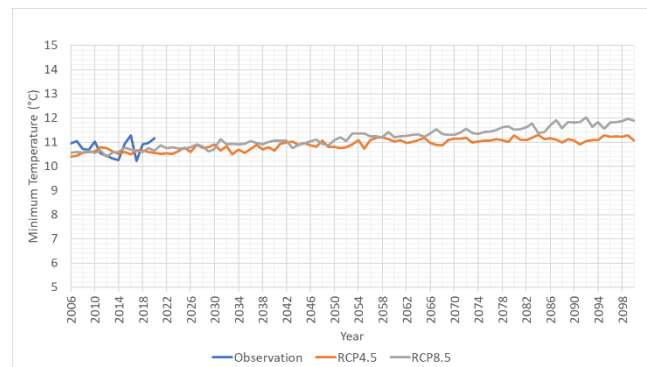

Figure 17. The observed, local climate models based on RCP4.5 and 8.5 for average annual minimum temperature (Tmin.) in Fukusaki Station (2006-2100)
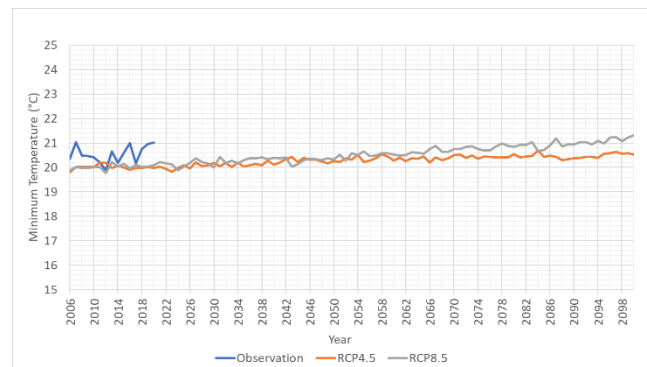

Figure 18. The observed, local climate models based on RCP4.5 and 8.5 for average maximum temperature (Tmax.) in Kamigoori Station (2006-2100)
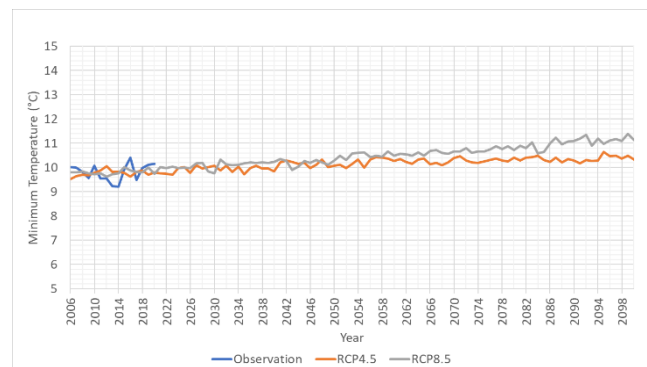

Figure 19. The observed, local climate models based on RCP4.5 and 8.5 for average annual minimum temperature of Kamigoori Station (2006-2100)

Table 9. Reliability assessment of maximum temperature models

Reliability test	RCP	R^2 ($R^2 \geq 0.4$)	Pearson Correlation ($r \geq 0.6$)	Cronbach's Alpha ($\alpha \geq 0.4$)
Toyooka (Northern)	4.5	0.965*	0.982*	0.991*
	8.5	0.967*	0.983*	0.992*
Sanda(South-western)	4.5	0.971*	0.985*	0.993*
	8.5	0.972*	0.986*	0.993*
Fukusaki (Southern)	4.5	0.970*	0.985*	0.993*
	8.5	0.973*	0.986*	0.994*
Kamigoori (South-eastern)	4.5	0.968*	0.984*	0.993*
	8.5	0.971*	0.985*	0.994*

indicates strong reliability.

Table 10. Reliability assessment of minimum temperature models

Reliability test	RCP	R^2 ($R2 \geq 0.4$)	Pearson Correlation ($r \geq 0.6$)	Cronbach's Alpha ($\alpha \geq 0.4$)
Toyooka (Northern)	4.5	0.973*	0.986*	0.993*
	8.5	0.973*	0.986*	0.993*
Sanda (South-western)	4.5	0.972*	0.986*	0.993*
	8.5	0.972*	0.986*	0.993*
Fukusaki (Southern)	4.5	0.974*	0.987*	0.992*
	8.5	0.976*	0.976*	0.993*
Kamigoori (South-eastern)	4.5	0.973*	0.987*	0.992*
	8.5	0.974*	0.987*	0.993*

indicates strong reliability.

There is a critical point which is the underestimation issues occur frequently in the selected stations. It might be due to the inability of SDSM to estimate extreme events which might result in lower temperature. Previous research has indicated that downscaling precipitation using the SDSM may not perform well since it may underestimate or exaggerate by omitting some extreme precipitation occurrences (Akhter, Shamseldin and Melville, 2019; Chin, Tan and Akihiko, 2021). Increasing trends are observed in all of the stations, where the increase of maximum values range between 0.3 °C to 1.3 °C. Based on the result, the increasing trends found in Tmax. and Tmin. model starting 2066 onwards for RCP8.5 scenario which is tallied in accordance to IPCC Sixth Assessment Report (AR6). This is due to higher emission scenario with GHGs reduction policy are not available in most of the countries after 2050. However, interested parties and government agencies from Japan should take the consideration that underestimation issue occurs in the simulated local climate models for temperature.

4. Conclusion

Local climate models based on RCP4.5 and RCP8.5 scenarios are successfully developed, and the reliability of models were assessed using linear regression, Pearson correlation and Cronbach alpha. Moderate relationships were obtained from the reliability assessments, where both local climate models simulated based on RCP4.5 and RCP8.5 scenarios showed similar valid and reliable results. Underestimation issues were found in all stations during Autumn seasons, which might be due to the failure of SDSM to project extreme rainfall intensity.

The simulated rainfall pattern in different regions of Hyogo Prefecture shows there is increased rainfall from 2021 – 2100 based on both RCP scenarios especially the local climate model for northern region of Hyogo shows significant increase of rainfall intensity. Besides, the southern region is expected to experience increase in rainfall (2021 – 2040), but the rainfall pattern is estimated to have slight fluctuations from 2041 – 2100. Both regions show different trends as they are in different climatic regions. However, local climate models based on RCP4.5 showed less significant increase in overall as compared to RCP8.5 scenario. Strong relationships were found between observed and simulated maximum and minimum temperature for RCP4.5 and RCP8.5 scenarios. Steady increase of average maximum and minimum temperature was observed from the simulated local climate models within the range of 0.3 °C to 1.3 °C. The range falls between the projected change in the average surface temperature by IPCC Sixth Assessment Report (AR6).

Locally, we suggested that relevant government agencies and interested parties should take initiative to develop the disaster risk reduction plan with integration of climate uncertainty. Besides, measures to reduce in greenhouse gas emissions such as afforestation and building design to reduce heat island effect shall be taken to stabilize the surface temperatures. However, continual climate modelling and improvement are suggested to monitor and project the changes in rainfall intensity and surface temperature.

References

Akhter M.S., Shamseldin A.Y., and Melville B.W. (2019). Comparison of dynamical and statistical rainfall downscaling of CMIP5 ensembles at a small urban catchment scale, *Stochastic Environmental Research and Risk Assessment*, **33**(4), 989–1012.

Beyer R., Krapp M. and Manica A. (2019). A systematic comparison of bias correction methods for paleoclimate simulations, *Clim. Past Discuss*, **11**, 1–23.

Brown J.D. (2002). The Cronbach alpha reliability estimate, *JALT Testing & Evaluation SIG Newsletter*, **6**(1), 17–19.

Chin K.S., Tan K.W. and Akihiko N. (2021). Development of statistically downscaled regional climate model based on representative concentration pathways for Ipoh, Subang and KLIA Sepang in Peninsular Malaysia, *IOP Conference Series: Earth and Environmental Science*, **945**(1), 012022.

DelSole T. and Shukla J. (2009). Artificial skill due to predictor screening, *Journal of Climate*, **22**(2), 331–345.

Domínguez M., *et al.* (2013). Present-climate precipitation and temperature extremes over Spain from a set of high resolution RCMs, *Climate research*, **58**(2), 149–164.

Frost J. (2021). *How to interpret R-squared in regression analysis*, accessed August **15**, 2021, https://statisticsbyjim.com/regression/interpret-r-squared-regression/.

Gogtay N.J. and Thatte U.M. (2017) Principles of correlation analysis, *Journal of the Association of Physicians of India*, **65**(3), 78–81.

Government of Canada. (2019). CanESM2 predictors: CMIP5 experiments, accessed August 14, 2021, https://climate-scenarios.canada.ca/?page=pred-canesm2.

IPCC. (2021). Summary for policymakers. *Climate Change The Physical Science Basis. Contribution of Working Group I to the Sixth Assessment Report of the Intergovernmental Panel on Climate Change*. Cambridge University Press. In Press.

Kang H. (2013). The prevention and handling of the missing data, *Korean Journal of Anesthesiology*, **64**(5), 402.

Maraun D. and Widmann M. (2018). *Statistical downscaling and bias correction for climate research*. Cambridge University Press.

McDonald J.H. (2014). *Handbook of biological statistics*. 3rd ed. Baltimore, Maryland: Sparky House Publishing.

Mikhaylov A., *et al.* (2020). Global climate change and greenhouse effect, *Entrepreneurship and Sustainability Issues*, **7**(4), 2897.

Mitas L. and Mitasova H. (1999). Spatial interpolation, *Geographical and Information Systems: Principles, Techniques, Management and Applications*, **1**(2).

National Aeronautics and Space Administration. (2021) 2020 tied for warmest year on record, NASA analysis shows, *NASA News*, accessed June **28**, 2021, https://climate.nasa.gov/news/3061/2020-tied-for-warmest-year-on-record-nasa-analysis-shows/.

Pidcock R. and McSweeney R. (2021). Mapped: how climate change affects extreme weather around the world. *Carbon Brief*, accessed June **29**, 2021, https://www.carbonbrief.org/mapped-how-climate-change-affects-extreme-weather-around-the-world.

UC Regents. (2021). What does Cronbach's alpha mean?, accessed April **10**, 2022, https://stats.oarc.ucla.edu/spss/faq/what-does-cronbachs-alpha-mean/.

Yang X., *et al.* (2015). Spatial interpolation of daily rainfall data for local climate impact assessment over greater Sydney region, *Advances in Meteorology*, **2015**, 1–12.